Design of quantum dot lattices in amorphous matrices by ion beam irradiation

M. Buljan, I. Bogdanović-Radović, M. Karlušić, U. V. Desnica, N. Radić, and M. Jakšić
Rudjer Bošković Institute, Bijenička cesta 54, HR-10000 Zagreb, Croatia

K. Salamon
Institute of Physics, Bijenička cesta 46, HR-10000 Zagreb, Croatia

G. Dražić
Jožef Stefan Institute, Jamova 39, SLO-1000 Ljubljana, Slovenia

S. Bernstorff
Sincrotrone Trieste, I-34149 Basovizza, Italy

V. Holý
Charles University in Prague, CZ-12116 Prague, Czech Republic
(Received 21 September 2011; published 17 October 2011)

We report on the highly controllable self-assembly of semiconductor quantum dots and metallic nanoparticles in a solid amorphous matrix, induced by ion beam irradiation of an amorphous multilayer. We demonstrate experimentally and theoretically a possibility to tune the basic structural properties of the quantum dots in a wide range. Furthermore, the sizes, distances, and arrangement type of the quantum dots follow simple equations dependent on the irradiation and the multilayer properties. We present a Monte Carlo model for the simulation and prediction of the structural properties of the materials formed by this method. The presented results enable engineering and simple production of functional materials or simple devices interesting for applications in nanotechnology.

DOI: 10.1103/PhysRevB.84.155312 PACS number(s): 81.07.Ta, 68.65.Ac, 81.15.Jj, 81.16.Dn

I. INTRODUCTION

Materials containing nanoparticles (NPs) or quantum dots (QDs) exhibit a remarkable range of properties,[1–7] which can be controlled by composition,[1,6,7] size,[6–8] and arrangement[9–11] of the QDs or NPs and by the matrix composition.[2] Therefore, such materials have numerous possible applications, especially in the field of photonics (lasers, sensors, photovoltaic devices, imaging, data storage, etc.)[12–21] and also as materials with enhanced thermoelectric efficiency.[22] Particularly interesting for various applications are semiconductor QDs and metallic NPs embedded in transparent, solid amorphous matrices. These matrices, like different kinds of glasses, usually have excellent optical, thermal, and mechanical properties, while QDs and NPs have easily manipulative confinement and plasmon-related effects or magnetic properties. However, the current control over the size and arrangement in three-dimensional (3D) arrays of QDs or NPs in such matrices is very limited, and controllable production of such materials is still under development.

Recently we have demonstrated a method to produce regularly ordered 3D arrays of QDs in amorphous matrix, which is based on ion beam irradiation (IBI) of an amorphous multilayer.[23,24] Here, we present surprisingly controllable structural properties of QDs formed by IBI. We show that the sizes of QDs and their distances and arrangement can be continuously tuned in a simple way, i.e., by tuning the angle that the ion beam makes with the multilayer surface. The tuning possibilities are even wider if various multilayer constructions and/or various ion types are used. Then, the size of the QDs and their separation and composition, as well as composition of the surrounding matrix, can be controlled in each layer of a multilayer separately. All our results and tuning possibilities are expressed by a set of simple equations and theoretically supported by a Monte Carlo model. The model is based on general assumptions, so it can be used for prediction of QD sizes and their arrangement properties for various materials.

II. PREPARATION

Multilayers containing twenty (Ge + SiO_2)/SiO_2 and (Ni + SiO_2)/SiO_2 bilayers [bilayer period P, Ge-rich (or Ni-rich) layer period p, and Ge:SiO_2 (Ni:SiO_2) molar ratios MR] were deposited by magnetron sputtering on a Si(111) or fused SiO_2 substrates at room temperature (RT) under the working gas pressure 0.7 Pa. Three types of multilayer samples with Ge were produced: (1) $P_1 = 15$ nm, $p_1 = 5$ nm, $MR_1 = 27:73$; (2) $P_2 = 10$ nm, $p_2 = 4$ nm, $MR_2 = 19:81$; (3) $P_3 = 6$ nm, $p_3 = 1.5$ nm, $MR_3 = 19:81$, and one multilayer type with Ni: (4) $P_4 = 10$ nm, $p_4 = 5$ nm, $MR_4 = 27:73$.

After the deposition, the multilayers were irradiated at RT by various ions (1 MeV O^{3+}, 3 MeV O^{3+}, 6 MeV Si^{3+}, 15 MeV Si^{4+}), at one of the four dosage values: $D_1 = 5 \times 10^{14}$, $D_2 = 1 \times 10^{15}$, $D_3 = 2 \times 10^{15}$, $D_4 = 4 \times 10^{15}$ ions/cm^2, and at one of the four ion beam incidence angles with respect to the multilayer surface: $\varphi_{irr} = 30°$, 45°, 60°, 90°. After the irradiation, the multilayers containing Ge were annealed for 1 h in vacuum at 800 °C. The sizes and arrangement of the resulting QDs are determined by scanning transmission electron microscopy (STEM) equipped with a high-angle annular dark-field detector (HAADF) and by grazing-incidence

small-angle x-ray scattering (GISAXS). The STEM images were obtained using a Jeol 2010F FEG-TEM/STEM microscope. The GISAXS measurements were performed using the SAXS beamline at synchrotron Elettra at photon energy of 8 keV. The optical absorption spectra were measured using a Perkin Elmer spectrometer.

III. RESULTS AND DISCUSSION

A. Ion-beam-assisted self-assembly

We investigate the size and arrangement properties of QDs formed by ion-beam-assisted self-assembly in amorphous multilayer films. For this purpose, fully amorphous (Ge + SiO_2)/SiO_2 and (Ni + SiO_2)/SiO_2 multilayer films with various layer thicknesses, produced by magnetron sputtering deposition, are irradiated by ion beams with various beam parameters [Fig. 1(a)] followed by thermal treatment. For the best self-assembly results, the parameters of the ion beam should be chosen to ensure approximately straight ion trajectories through the multilayer and the transfer of energy to the surrounding material mainly by electronic stopping (S_e), i.e., by inelastic collisions of ions with the electrons bounded in the multilayer.[25] For this purpose, the level of S_e needs to be in the range of approximately 1.5–3 keV/nm for the amorphous silica matrix. If the S_e is too low ($S_e = 1.03$ keV/nm with the 1 MeV O^{3+} beam), the effect is hardly observed; if Se is too high ($S_e = 4.6$ keV/nm with the 15 MeV Si^{4+} beam), the multilayer begins to be destroyed. The range of the ions is typically on the order of a μm far exceeding the total film thickness; therefore, other effects [e.g., elastic collisions with nuclei in the target material (S_n)] that may become dominant near the end of the trajectory can be neglected for the multilayer thicknesses investigated in this work. The 3 MeV O^{3+} ions

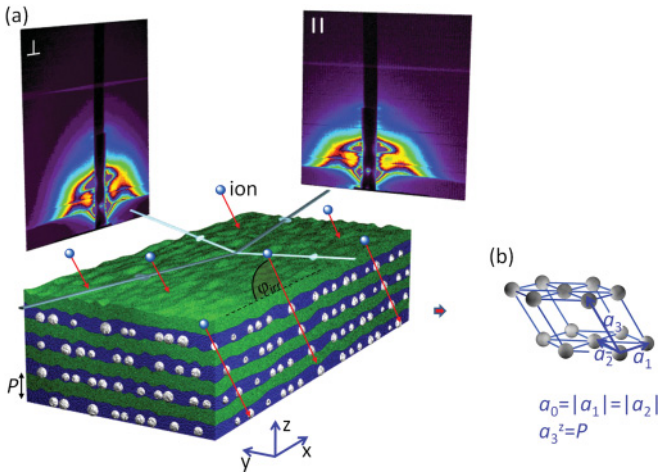

FIG. 1. (Color online) (a) The initially amorphous multilayer (bilayer thickness P) is irradiated by an ion beam incident at angle φ_{irr} with respect to the film surface; the red arrows indicate the irradiation direction. The irradiation incites the formation of regularly ordered QDs (white spheres). Structural measurements were performed for parallel (||) and perpendicular (⊥) configurations (indicated by gray arrows), showing the relation of the probing beam and the irradiation direction. (b) Description of the QD lattice formed by ion beam irradiation.

($S_e = 1.8$ keV/nm, $S_n = 0.01$ keV/nm) were found to be optimal for the design of QD lattices.

Passing through the material, ions slow down due to inelastic electron scattering.[26] The lost kinetic energy is deposited in the surrounding material, causing a temporary increase of temperature T within a cylindrical region around the ion trajectory called the ion track.[26–30] The width of the ion track w represents the region where the temperature increase is high enough to cause significant changes in the material (i.e., nucleation and growth of QDs). This local increase of T incites the formation of nuclei of QDs and/or promotes the growth of already existing ones within the ion track, when the parameters of the ion beam are properly chosen (see Sec. II). We will show that the sizes and arrangement of the formed QDs are highly influenced by the properties of ion beam and that they may be easily tuned in a large range. Post-irradiation annealing is applied to finish the growth process of the QD nuclei and their crystallization, and to remove the radiation damage.[24] The final result is the formation of three-dimensionally (3D) ordered crystalline Ge QDs in amorphous silica matrix [see Fig. 1(b)].

B. Simple rules for basic structural properties

A 3 MeV O^{3+} ion beam is found to be optimal for the production of ordered QD arrays in the Ge + SiO_2 system (for more details see Sec. II); therefore, we demonstrate here its application on the design of QD lattices. Structure of the multilayers is studied by comparative STEM GISAXS analysis. Several examples of the structure of the (Ge + SiO_2)/SiO_2 multilayers after IBI and annealing are depicted in Fig. 2, while the systematic analysis is shown later. The irradiation with sufficiently large dose of O^{3+} ions, followed by thermal annealing, causes formation of QDs along approximately straight lines [Figs. 2(a)–2(c)] running at angle φ_{corr} with respect to the sample surface. The ordering is clearly visible especially in the Fourier transformations (FTs) of the STEM images [insets of Figs. 2(a)–2(c)] and in the GISAXS maps of the films [Figs. 2(d)–2(f)], where the spatial correlation (ordering) of the QD positions is manifested as strong, diffraction-like maxima with the tilt angle φ_{corr} with respect to the normal to the sample surface (indicated by red lines in Fig. 2). GISAXS[31] is especially suitable for the analysis of such a system since it is nondestructive, provides data with excellent statistics, and enables a very precise determination of the QD size, shape, and arrangement. The precise determination of these parameters is performed using a model[24,32] describing the GISAXS from the irradiated multilayers. The simulations of the measured maps are shown in the insets of Figs. 2(d)–2(f).

The first important feature of the grown QD lattices is the relation between the correlation angle φ_{corr} and the irradiation angle φ_{irr}. The preferential QD ordering shown in Figs. 2(a), 2(b), 2(d), and 2(e) coincides with the irradiation direction, i.e., $\varphi_{corr} = \varphi_{irr}$. This phenomenon occurs if relatively high ion doses and high incidence angles are applied. For the combination of low doses and low incidence angles, the irradiation and correlation angles are quite different [Figs. 2(c) and 2(f)].

Another important effect is the tunability of the QD size and of the in-layer QD spacing a_0 [Fig. 1(b)] by suitable selection

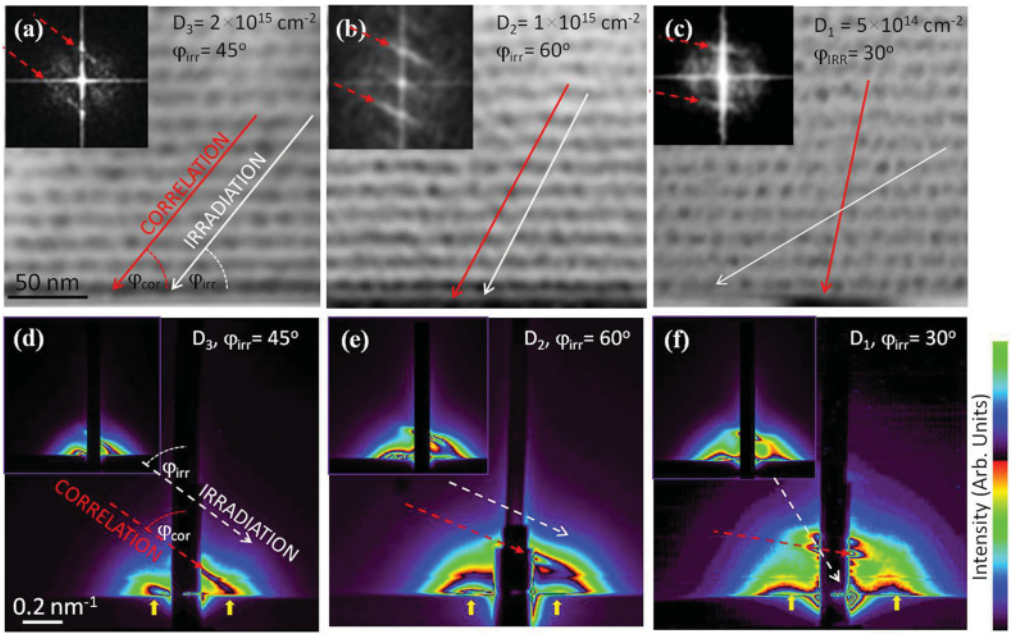

FIG. 2. (Color online) Structure of the irradiated and annealed multilayers of (Ge + SiO_2)/SiO_2. (a)–(c) Examples of STEM cross sections of the same type of multilayers ($P = 15$ nm) irradiated by a 3 MeV O^{3+} ion beam under various conditions indicated in the figure. The insets show the FT of the STEM images. The directions of ion irradiation and of the correlation of the dot positions are shown by white and red arrows, respectively. (d)–(f) The corresponding GISAXS maps measured in ⊥ configuration. The insets show simulated GISAXS maps, obtained by fitting of the experimental data. The lateral intensity maxima (so-called Bragg spots) stemming from the in-plane correlation of the dot positions are indicated by yellow arrows.

of the irradiation parameters. This feature is clearly visible in the GISAXS maps of the multilayers [Figs. 2(d)–2(f)]: A decrease in the QD size causes an increase in the radius of the semicircular intensity background, while a decrease in a_0 causes an increase in the spacing between the lateral Bragg spots. Thus, the largest values of the QD size and a_0 are found for the multilayers presented in Figs. 2(a) and 2(d) while the smallest values are in the multilayers in Figs. 2(c) and 2(f).

To summarize, the QD correlation angle, QD sizes, and QD in-layer spacing a_0 depend on the irradiation conditions. In the following, we present a systematic quantitative analysis of all structural parameters obtained by the irradiation of the same type of multilayer films with different doses and under different irradiation angles. The correlation angle φ_{corr} [Fig. 3(a)], in-layer lattice parameter a_0 [Fig. 3(b)], and mean QD radius R [Fig. 3(c)] are examined. The values of the structural parameters are obtained by numerical analysis of GISAXS maps using the model presented in Ref. 24; the results are in excellent agreement with the STEM results.

All structural properties in Fig. 3 show a strong and systematic dependence on the irradiation conditions. The properties can be tuned in a large range by a simple change of the irradiation angle. However, the most remarkable point of the observed properties is the fact that the dependencies for the high irradiation doses (D_3 and D_4) can be well described by the following set of simple equations (dotted lines in Fig. 3):

$$\varphi_{\mathrm{corr}} = \varphi_{\mathrm{irr}}, \tag{1}$$

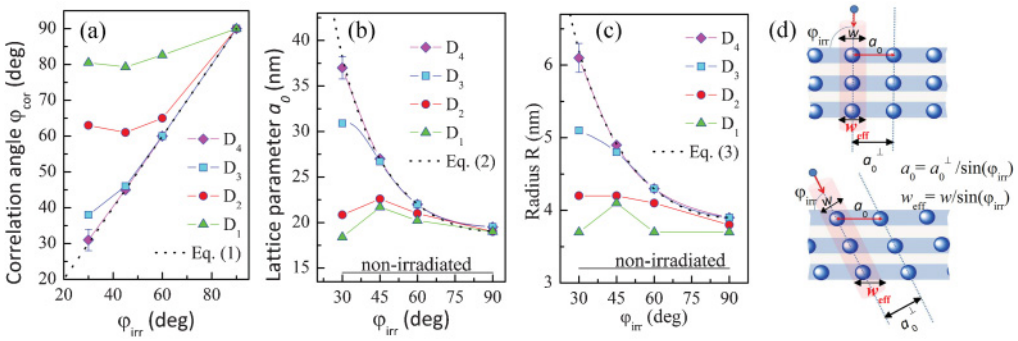

FIG. 3. (Color online) Dependence of the QD arrangement and size parameters on the irradiation conditions: (a) correlation angle φ_{irr}, (b) in-layer QD lattice parameter a_0, and (c) mean QD radius R. Theoretical values given by Eqs. (1)–(3) are shown as the black dotted line. The root mean square deviations of the measured values are shown by error bars. (d) Sketch of the change in the in-layer lattice parameter a_0 and effective width of ion track w_{eff} with the irradiation angle.

$$a_0 = a_0^{\perp}/\sin(\varphi_{\text{corr}}), \tag{2}$$

$$R = Ca_0^{2/3} = R^{\perp}/\sin(\varphi_{\text{corr}}), \tag{3}$$

where $a_0^{\perp}$ is the in-layer QD spacing for the normal incidence of irradiating ions ($\varphi_{\text{irr}} = 90°$). The value of $a_0^{\perp}$ is found to be determined entirely by the width of the ion track w, as will be shown later. C is a constant determined by the Ge volume fraction in the Ge-rich layers (η) and by the Ge + SiO_2 layer thickness (p) according to $C = (\eta\frac{3^{3/2}p}{8\pi})^{1/3}$, and $R^{\perp}$ is the QD radius obtained for $\varphi_{\text{irr}} = 90°$. Equation (1) reflects the experimental observation that the correlation direction approaches the irradiation direction for sufficiently large doses. Equation (2) is based on the assumption that the in-layer QD spacing is proportional to the width of the ion track in the direction parallel to the multilayer [Fig. 3(d)]: $w_{\text{eff}} = w/\sin(\varphi_{\text{irr}})$. Finally, Eq. (3) for the QD radius is derived under the assumption that the volume of a QD is proportional to the volume of the portion of the Ge-rich layer belonging to a single QD in the QD lattice. All results are very well reproducible.

For smaller ion doses D_1 and D_2, a similar tendency of the parameter behaviors is observed but the aforementioned effects tend to decrease. When the irradiation dose and/or the irradiation angle is decreased, the correlation angle does not reach the irradiation angle and all the parameter values approach the values obtained for the case with no irradiation. This finding is expected since the value of a_0 would become much larger than the intrinsic (non-irradiated) spacing of QDs for small φ_{irr}, according to Eq. (2) [Fig. 3(b)], so a higher dose is needed to produce the full effect.

The statistical distribution (root mean square deviations) of the QD in-layer spacing is significantly improved by the irradiation treatment. It decrease from the initial 35% of the lattice parameter value a_0 for the non-irradiated case, to about 20% for the smallest irradiation dose D_1. The increase of the dose leads to the further improvement to nearly 15% for the highest irradiation dose D_4. The deviation of QD positions from the correlation direction defined by φ_{corr} is about 20% for the lowest dose and 10% for the highest one. The deviations of the vertical positions of the QDs are small (below 0.5%) because QDs are formed within the Ge-rich layers, and they do not change their vertical position during the irradiation. The standard deviation of the size distribution is about 20% of the QD radius for the lowest dose and about 15% for the highest one. The deviation parameters are estimated by using of numerical analysis of the GISAXS intensity distributions.

C. Modeling and design of QD lattices: Monte Carlo simulations

The observed phenomena can be explained in terms of the interaction of ions with the multilayers. As described previously, the ion passage through the multilayer produces a temperature increase within the ion track.[29,30] The amplitude and duration of this increase may be adjusted by the proper choice of ion beam parameters. In this way, the adequate conditions are ensured for the nucleation and growth of the QDs with specific composition. The tunability of the structural properties of the QD lattice is achieved by the effective width of the ion track w_{eff}, defined as the width of the ion track in the direction parallel to the multilayer; it can be easily tuned by the irradiation angle: $w_{\text{eff}} = w/\sin(\varphi_{\text{irr}})$.

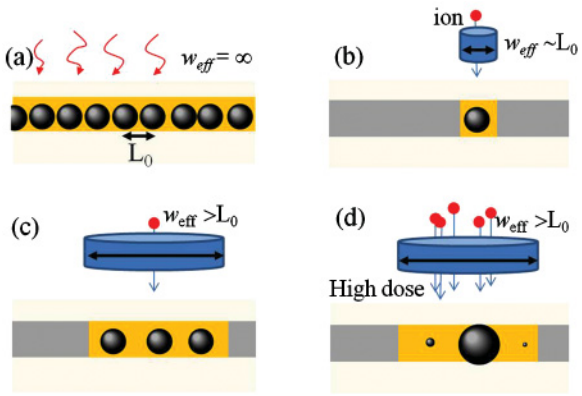

FIG. 4. (Color online) (a) Standard thermal annealing. The intrinsic separation of the QDs is L_0. (b) Effect of a single ion when the width of its track is comparable to L_0. A nucleation of a single QD within the track volume is possible. (c) Irradiation by a single ion if the ion track is broader than L_0; several QDs with the mean separation of L_0 can be created in the irradiated volume. (d) Influence of a high irradiation dose; the Ostwald ripening process takes place.

To explain the observed dependencies on the irradiation dose and angle, we follow the influence of the temperature-induced changes in the multilayer, schematically illustrated in Fig. 4. The multilayer before the temperature increase (irradiation or annealing) consists of homogeneous Ge-rich layers (without any QDs formed) separated by pure matrix layers.[24] When a standard thermal annealing is applied without a prior irradiation [Fig. 4(a)] Ge QDs are formed within the entire Ge-rich layer by a diffusion-mediated nucleation. Then, the QDs formed are distributed randomly within the Ge-rich layers with the intrinsic average separation of L_0, determined by the multilayer and annealing parameters.[33] Thus, the depletion regions with the mean radius L_0 are formed around each nucleus during its growth, reducing the probability of nucleation of another QD inside them. Similar processes occur inside the ion tracks in picosecond time scales. When the multilayer is irradiated by an ion producing an ion track with the effective width of w_{eff} smaller or comparable to the intrinsic QD separation ($w_{\text{eff}} \leqslant L_0$), a single Ge nucleus will form [Fig. 4(b)] within it. On the other hand, if the ion track is much wider than the intrinsic QD separation ($w_{\text{eff}} \gg L_0$), several nuclei (separated by some value close to the intrinsic spacing) can be formed within the irradiated volume [Fig. 4(c)].

If more than one ion is applied, each new ion causes a new nucleation or promotes the growth of already existing nuclei within the ion track. If the dose is small, the separation of QDs is not far from the intrinsic value due to the formation of depletion regions. An increase of the dose causes the growth of the nuclei and the concentration of free Ge atoms becomes smaller. If the dose is sufficiently large, a transfer of Ge atoms from smaller QDs to the larger ones becomes significant [Ostwald ripening process; Fig. 4(d)], leading to the survival of a single QD within the width of the ion track. For large doses, therefore, the final spacing of QDs is mainly determined by w_{eff}.

The ripening process continues during the post-irradiation annealing. This process takes place simultaneously throughout the entire film and causes the dissolution of the remaining, very small Ge clusters, the homogenization of the QD spacings and sizes (w_{eff} is approximately equal in all directions parallel to the substrate after annealing), and finally, the crystallization of the Ge QDs. The homogenization occurs due to the dependence of the transfer rate during the ripening process on the QD spacing.

We have developed a Monte Carlo model based on the above-mentioned assumptions in order to predict and simulate the structure of QD lattices. The main assumption of the model is that the passage of an ion causes an increase in local temperature T within the ion track.[26–30] The increase of T and hence the width of the ion track (w) are determined by the amount of energy loss of the incoming ion and by the thermodynamic parameters of the multilayer. The cylindrically shaped temperature distribution within the ion track is given by

$$T(r,t) = T_0 + Q(t)\exp\left[-\frac{[x - x_0 + (z - z_0)/\tan(\varphi_{\text{irr}})]^2}{w_x(t)^2} - \frac{(y - y_0)^2}{w_y(t)^2}\right], \tag{4}$$

where T_0 is the temperature at which the irradiation is performed, $\boldsymbol{r} = (x,y,z)$ is the position coordinate, $\boldsymbol{r}_0 = (x_0,y_0,z_0)$ denotes the center of the ion track at the multilayer surface, and t is the time. The three time-dependent functions,

$$w_x(t) = \begin{cases} \frac{w_0 t_0^{1/2}}{\sin(\varphi_{\text{irr}})}, & t \leqslant t_0, \\ \frac{w_0 t^{1/2}}{\sin(\varphi_{\text{irr}})}, & t > t_0, \end{cases} \quad w_y(t) = \begin{cases} w_0 t_0^{1/2}, & t \leqslant t_0, \\ w_0 t^{1/2}, & t > t_0, \end{cases}$$
$$Q(t) = \begin{cases} T_{\max}\frac{t}{t_0}, & t \leqslant t_0, \\ T_{\max}\frac{t_0}{t}, & t > t_0, \end{cases} \tag{5}$$

describe the propagation of heat within the material, where $T_{\max}$ is the temperature increase peak, t_0 is the time when the temperature inside the ion track is the highest, and w_0 is a parameter determined by the material properties. The irradiation direction is placed in the x-z plane. The peak temperature is $T_{\max} = S_e g/(\pi\rho c w_0^2 t_0)$ according to Ref. 30, where S_e is the value of electronic stopping in the material determined by SRIM calculation,[25] g is the efficiency in energy transfer from an electron to the phonon system, and ρ and c are the density and specific-heat capacity of the material, respectively.[30] For pure amorphous SiO_2, $g = 0.4$, $\rho = 2.2$ g/cm^3, $c = 700$ J/kg K, and $w_0 t_0^{1/2} = 3.4$ nm (Ref. 28), whereas S_e depends on the properties of both ion and material; for O^{3+} ions $S_e = 1.68$ keV/nm (Ref. 25). These parameters are slightly modified by the presence of Ge in the Ge-rich layers.

The temperature increase incites the diffusion of Ge atoms inside the ion track. The result of the enhanced diffusion is the formation and/or growth of Ge nuclei within the track. The profile of the Ge concentration ρ_{Ge} around each nucleus is found numerically by solving the 3D diffusion equation

$$\frac{\partial \rho_{\text{Ge}}(\boldsymbol{r},t)}{\partial t} = \nabla[D_{\text{Ge}}(\boldsymbol{r},t)\nabla\rho_{\text{Ge}}(\boldsymbol{r},t)], \tag{6}$$

where $D_{\text{Ge}}(r,t)$ is the diffusion coefficient of Ge atoms $D_{\text{Ge}}(\boldsymbol{r},t) = D_0\exp\{-E_{\text{ac}}/[k_B T(\boldsymbol{r},t)]\}$, E_{ac} is the activation energy for Ge diffusion, and D_0 is the diffusion prefactor.

We used a simplified model, based on the basic nucleation theory[33–35] and Eqs. (4)–(6), in order to describe the growth of QDs and the time evolution of the depletion region around each dot. The process of nucleation is simplified by assuming that only supercritical nuclei with spherical shape and the radius $R \geqslant R_{\text{crit}}$ appear. The model further assumes the formation of nuclei within the ion track, each accompanied by a surrounding depletion region with a decreased Ge density and zero probability of nucleation of additional dots. The number of Ge inclusions actually created in the ion track depends on $w_{\text{eff}} = w/\sin(\varphi_{\text{irr}})$ and on the radius $R_{\text{depl}} = L_0$ of the depletion region. This radius corresponds to the mean spacing L_0 of QDs in an annealed, non-irradiated Ge + SiO_2 layer, introduced above. The profile of the Ge density in the depletion region is determined according to Ref. 34, taking into account the conservation of the total Ge amount. If R_{depl} is comparable to w_{eff}, only a single inclusion grows in the center of the track. If $w_{\text{eff}} \gg R_{\text{depl}}$, several short-range ordered inclusions occur since the mean spacing between inclusions is dependent on R_{depl}.

Finally, we consider a possible degradation of existing nuclei via an Ostwald-ripening-like process. When the concentration of free Ge atoms is small, the transfer of atoms already incorporated in one QD to another QD (ΔN) in the

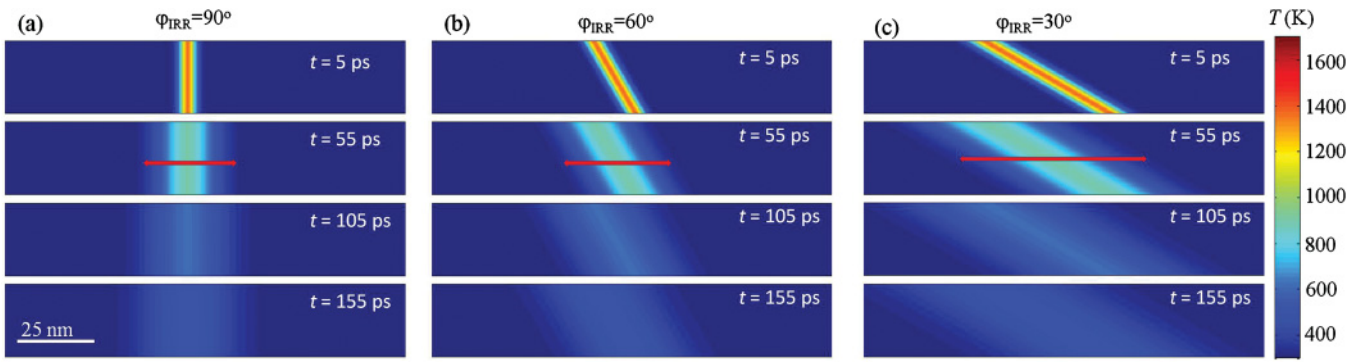

FIG. 5. (Color online) Time evolution of the temperature in the film during the ion passage through it. (a) Irradiation angle $\varphi_{\text{irr}} = 90^\circ$, (b) $\varphi_{\text{irr}} = 60^\circ$, (c) $\varphi_{\text{irr}} = 30^\circ$. The time t is indicated in each panel. Decreasing the irradiation angle causes increase of the effective width of the ion track (denoted by red arrows).

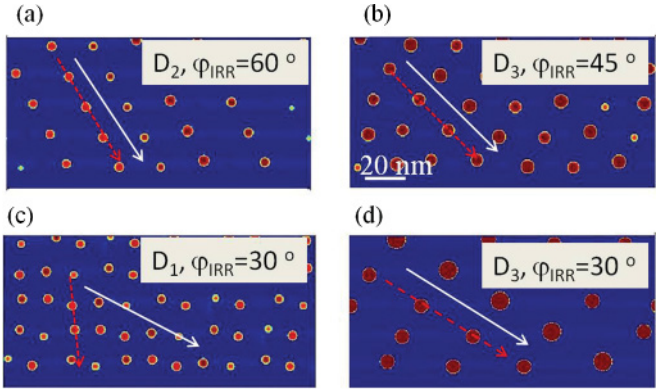

FIG. 6. (Color online) (a)–(c) Simulations of the structural properties of the films obtained from TEM cross sections presented in Figs. 2(d)–2(f). (d) Simulation of the QD arrangement for large dose and small irradiation angle under the influence of the Ostwald ripening illustrated in Fig. 4(d). The irradiation and correlation directions are denoted by white and red arrows, respectively.

time step Δt is described by the standard formula for the ripening process,[35] namely,

$$\frac{\Delta N}{\Delta t} = \text{const.}\frac{A}{d_{R,R'}}\left(\frac{1}{r}-\frac{1}{R'}\right) \times \min[D_{\text{Ge}}(r=R,t), D_{\text{Ge}}(r=R',t)], \qquad (7)$$

where R and R' are the radii of the neighboring QDs, $d_{RR'}$ is their spacing, A is the area of the interaction cross section,[35] and the minimum factor expresses the minimum value of the diffusion coefficient on the surfaces of the neighboring quantum dots.

Post-deposition annealing at $T_a = 800\,^{\circ}\text{C}$ for $t = 1$ h is simulated by using the alternative steps for nuclei growth and Ostwald ripening (items 4 and 5 of the Appendix).

We have performed extensive numerical simulations following the above strategy. For each irradiation angle and for each ion we calculate the temperature evolution inside the film using Eqs. (4) and (5). The temperature evolutions caused by the passage of a single ion at various incidence angles is shown in Fig. 5. From the figure the spreading of the temperature in time is evident. As well, the dependence of the ion track width in the direction parallel to the multilayer surface on the irradiation angle is indicated in Fig. 5. Using the temperature at a given time step, the diffusion coefficient of Ge was calculated and the diffusion equation was solved, as described above. Following the algorithm given in Appendix we have simulated the experimentally measured structural properties of the films. The simulation results [Figs. 6(a)–6(c)] agree very well with the experimental data [Figs. 2(a)–2(c)] for all doses and irradiation angles (and also for all other experimental data not shown here). The nucleation and growth process induced by the irradiation is compared to the same process induced by thermal effect without irradiation.[36] The nucleation and growth of Ge clusters is found for temperatures $T > 250\,^{\circ}\text{C}$.[36] Approximately the same limiting temperature is found important for Ge clustering within the ion tracks. This result is expected because the diffusion coefficient of Ge becomes significant for those temperatures and nucleation and growth of Ge clusters may occur.

The more interesting point is the fact that the spacing of QDs formed by the irradiation is determined by the maximal width of the ion track at $T \approx 250\,^{\circ}\text{C}$ ($w_{T=250}$) for a sufficiently large dose. This is a consequence of the ripening process; the ripening process caused by a single ion is possible only within the track where $T > 250\,^{\circ}\text{C}$. Therefore, the minimal separation of QDs equals $w_{T=250}$ for the final stage of ripening when only a single QD survives within the ion track. Similarly, the maximal separation is $2 \times w_{T=250}$. The average separation of QDs is between these two limiting cases; for our experimental data it is roughly $1.5 \times w_{T=250}$.

In summary, the in-layer spacing of QDs is determined by w_{eff} for the higher doses, and it changes according to Eq. (7) due to the ripening process.

IV. DISCUSSION

The presented data show the possibility for a continuous tuning of the properties of QD lattices and QD sizes over a large range only by varying the irradiation angle. The possible range of tuning is even wider if we use ion beams and/or multilayers with various properties. By changing the energy or type of ions we change the width of the ion track, i.e., the

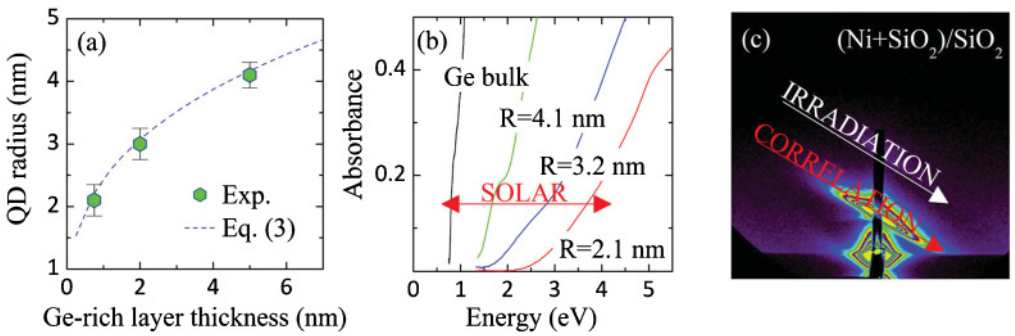

FIG. 7. (Color online) (a) Change in the QD size with the varying thickness of Ge-rich layers (dose D_2, $\varphi_{\text{irr}} = 60^{\circ}$). The dependence following from Eq. (3) is shown by the blue dashed line. The layer thicknesses are corrected to include the effects of slightly different Ge:SiO_2 molar ratios. (b) Optical absorbance of the films with various layer thicknesses, irradiated under the same conditions (dose D_2, $\varphi_{\text{irr}} = 60^{\circ}$) producing Ge QDs of various sizes (indicated in the figure). The red arrow indicates the energy range of solar spectrum. (c) GISAXS map showing the self-assembly of Ni NPs in (Ni + SiO_2)/SiO_2 multilayer (dose D_2, $\varphi_{\text{irr}} = 60^{\circ}$).

temperature distribution within it, so we are able to vary the in-plane QD spacing a_0. On the other hand, the thickness of the Ge-rich layer has a decisive effect on the QD sizes. Namely, the dot size is rapidly increasing with the thickness of Ge-rich layers [Fig. 7(a)]. This fact may be used for the manipulation of optical properties of the material via the charge carrier confinement; this effect is especially strong in Ge QDs.[8] It is important to note that the thicknesses of the individual Ge-rich layers in a multilayer may be freely chosen, which makes it possible to control the QD sizes in each individual layer separately. Thus, combining layers with various thicknesses, it is easy to construct materials with graded band gaps, covering the whole range of the solar spectrum [Fig. 7(b)], for instance, which are important for optoelectronic devices such as solar cells.

The application range can be further broadened if the material of the multilayer is varied. We have irradiated multilayers containing metal (Ni) atoms instead of Ge, and the aforementioned self-assembly effect was achieved even more easily [Fig. 7(c)], i.e., with smaller doses and lower ion energies than for the case of Ge. Ni nanoparticles produced in this way are elongated along the ion tracks, and their aspect ratio can be tuned by the direction of the irradiation. This property can be used in the manipulation of plasmon-related effects and of the magnetic properties of the material.[37]

V. CONCLUSIONS

We have developed a method for a manipulation of the distances and sizes of self-organized nanoparticles in amorphous matrix. The presented results have a great potential as a new method for design and facile production of nano-based functional materials. The set of simple rules presented here enables the prediction of the sizes of nanoparticles and their spacing and arrangement in the matrix, while the materials can be freely chosen. They make it possible to control the quantum confinement effects, surface plasmons, and magnetic properties or collective behavior features that appear due to a regular arrangement of the particles. The assumptions of the developed model are quite general because they are based on a standard, temperature-driven nucleation that is well established for a wide class of materials. We proved that the method is valid both for Ge and Ni nanoparticles, and we expect a similar behavior for all materials in which nanoparticles can be produced by a diffusion-mediated nucleation.

ACKNOWLEDGMENTS

The authors acknowledge Hrvoje Buljan for help in developing the model for describing QD ordering. The authors are grateful to Medeja Gec for preparing samples for TEM measurements and to Aleksa Pavlešin for the assistance during sample preparation. M.B. acknowledges support from the Croatian Ministry of Science Higher Education and Sport and the European Science Foundation (SimBioMa program), V.H. acknowledges support from the Czech Science Foundation (Project No. P204-11-0785), and G.D. acknowledges support from the Slovenian Research Agency (P2-0084).

APPENDIX

The growth algorithm consists of the following steps:

(1) At time $t = 0$, we set the initial Ge concentration to a constant value ρ_{Ge}^{0} in a given volume (that is the concentration of homogeneously distributed Ge atoms in Ge-rich layer) and define nucleation conditions (nucleation occurs if $T > T_{\mathrm{crit}}$, $\rho > \rho_{\mathrm{crit}}$).

(2) We define a position $(x_0, y_0, z_0 = \text{const.})$ on the multilayer surface specifying the origin of an ion track, using a two-dimensional random position generator. The temperature distribution within the track for a given time step $(t + \Delta t)$ is calculated using Eqs. (4) and (5). The diffusion constant $D_{\mathrm{Ge}}(\boldsymbol{r},t)$ is calculated using the obtained temperature distribution.

(3) If there are no preexisting nuclei and no depletion regions within the track where nucleation conditions are fulfilled, a new Ge nucleus with radius R_{crit} is formed. Ge concentration inside the nuclei ($\rho_{\mathrm{Ge}}^{\mathrm{inside}}$) is assumed equal to Ge bulk density. Each nucleus is accompanied by a depletion region with the radius R_{depl}; we assume a Gauss-like decay of ρ_{Ge} at the boundaries of depletion regions toward the surface of the formed nuclei (number of Ge atoms must be conserved). The same procedure is repeated until nucleation is no longer possible under the given conditions.

(4) We solve the above-described diffusion model in Eq. (6) using the previous concentration distribution ρ_{Ge} as a starting condition. We obtain the Ge concentration $\rho_{\mathrm{Ge}}(\boldsymbol{r},t + \Delta t)$ after time step Δt. The increase of the number of Ge atoms (ΔN) per unit time in a nuclei (cluster) within the ion track equals the number of Ge atoms reaching the surface of the existing nuclei (ΔN) per unit time: $\frac{\Delta N}{\Delta t} = \rho_{\mathrm{Ge}}(r \leqslant R)$, where R is the radius of the nuclei (cluster) at time t.

(5) If the concentration of free Ge atoms is smaller than a certain critical value, then Ostwald ripening takes place according to Eq. (7).

(6) We repeat steps 2 to 5 for all successive time steps δt and for each ion in the given dose D.

The parameters used for the simulation of the irradiation with O^{3+} ions are the following: $\rho_{\mathrm{Ge}}^{0} = 5$ Ge atoms/nm^3, $\rho_{\mathrm{Ge}}^{\mathrm{inside}} = 44.5$ Ge atoms/nm^3, $T_{\mathrm{crit}} = 500$ K, $\rho_{\mathrm{crit}} = 1$ Ge atom/nm^3, $S_e(3\ \mathrm{MeV\ O}) = 1.674$ keV/nm [we have used $\rho(\mathrm{SiO_2} + \mathrm{Ge}) = 2.5$ g/cm^3 for calculation of S_e], $(T_{\max}\ 3\ \mathrm{MeV\ O}) = 1180$ K; $T_0 = 300$ K, $w_0 t_0^{1/2} = 4.4$ nm; $t_0 = 1 \times 10^{-12}$ s, $E_{\mathrm{ac}} = 1.0$ eV, $D_0 = 0.12$ cm^2/s, $R_{\mathrm{crit}} = 0.64$ nm, and $R_{\mathrm{depl}} = L_0 = 12$ nm.

[1] A. P. Alivisatos, Science **271**, 933 (1996).
[2] W. A. Murray and W. L. Barnes, Adv. Mater. **19**, 3771 (2007).
[3] R. Hanson, L. P. Kouwenhoven, J. R. Petta, S. Tarucha, and L. M. K. Vandersypen, Rev. Mod. Phys. **79**, 1217 (2009).

[4]F. H. Julien and A. Alexandrou, Science **282**, 1429 (1998).
[5]F. Xiu, Y. Wang, J. Kim, A. Hong, J. Tang, A. P. Jacob, J. Zou, and K. L. Wang, Nature Mater. **9**, 337 (2010).
[6]W. D. A. M. de Boer, D. Timmerman, K. Dohnalová, I. N. Yassievich, H. Zhang, W. J. Buma, and T. Gregorkiewicz, Nature Nanotechnology **5**, 878 (2010).
[7]L. Brus, J. Phys. Chem. **90**, 2555 (1986).
[8]C. Bostedt, T. van Buuren, M. Willey, N. Franco, and L. J. Terminello, Appl. Phys. Lett. **84**, 4056 (2004).
[9]A. Courty, A. Mermet, P. A. Alboy, E. Duval, and M. P. Pileni, Nature Mater. **4**, 395 (2005).
[10]D. Grützmacher, T. Fromherz, C. Dais, J. Stangl, E. Müller, Y. Ekinci, H. H. Solak, H. Sigg, R. T. Lechner, E. Wintersberger, S. Birner, V. Holý, and G. Bauer, Nano Lett. **7**, 3150 (2007).
[11]M. Buljan, U. V. Desnica, G. Dražić, M. Ivanda, N. Radić, P. Dubček, K. Salamon, S. Bernstorff, and V. Holý, Nanotechnology **20**, 085612 (2009).
[12]D. K. Gramotnev and S. I. Bozhevolnyi, Nature Photonics **4**, 83 (2010).
[13]G. E. Jabbour and D. Doderer, Nature Photonics **4**, 604 (2010).
[14]W. L. Barnes, A. Dereux, and T. W. Ebbesen, Nature (London) **424**, 824 (2003).
[15]Y. Liu, M. Gibbs, J. Puthussery, S. Gaik, R. Ihly, H. W. Hillhouse, and M. Law, Nano Lett. **10**, 1960 (2010).
[16]M. Kroutvar, Y. Ducommun, D. Heiss, M. Bichler, D. Schuh, G. Abstreiter, and J. J. Finley, Nature (London) **432**, 81 (2004).
[17]T. D. Ladd, F. Jelezko, R. Laflamme, Y. Nakamura, C. Monroe, and J. L. O'Brien, Nature (London) **464**, 45 (2010).
[18]Z. Mi, J. Yang, P. Bhattacharya, G. Qin, and Z. Ma, Proc. IEEE **97**, 1239 (2009).
[19]V. I. Klimov, A. A. Mikhailovsky, S. Xu, A. Malko, J. A. Hollingsworth, C. A. Leatherdale, H.-J. Eisler, and M. G. Bawendi, Science **290**, 314 (2000).
[20]G. Konstantatos and E. H. Sargent, Nature Nanotechnology **5**, 391 (2010).
[21]L. Zhang and T. J. Webster, Nano Today **4**, 66 (2009).
[22]S. Budak, J. Chacha, C. Smith, M. Pugh, K. Heidary, R. B. Johnson, and D. Ila, Nucl. Instrum. Methods B, doi: 10.1016/j.nimb.2011.04.090 (to be published 2011).
[23]M. Buljan, I. Bogdanović-Radović, M. Karlušić, U. V. Desnica, G. Dražić, N. Radić, P. Dubček, K. Salamon, S. Bernstorff, and V. Holý, Appl. Phys. Lett. **95**, 063104 (2009).
[24]M. Buljan, I. Bogdanović-Radović, M. Karlušić, U. V. Desnica, N. Radić, N. Skukan, G. Dražić, M. Ivanda, O. Gamulin, Z. Matej, V. Valeš, J. Grenzer, T. W. Cornelius, H. T. Metzger, and V. Holý, Phys. Rev. B **81**, 085321 (2010).
[25]J. F. Ziegler, J. P. Biersack, and U. Littmark, *The Stopping and Range of Ions in Solids* (Pergamon Press, New York, 1985; new edition in 2009).
[26]M. Toulemonde, C. Trautmann, E. Balanzat, K. Hjort, and A. Weidinger, Nucl. Instrum. Methods B **216**, 1 (2004).
[27]L. R. Fleischer, P. B. Price, and R. M. Walker, *Nuclear Tracks in Solids: Principles and Applications* (University of California Press, Berkeley, CA, 1975).
[28]M. L. Brongersma, E. Snoeks, and A. Polman, Appl. Phys. Lett. **71**, 1628 (1997).
[29]J. Jensen, A. Razpet, M. Skupinski, and G. Possnert, Nucl. Instrum. Methods B **245**, 269 (2006).
[30]G. Szenes, Phys. Rev. B **51**, 8026 (1995).
[31]G. Renaud, R. Lazzari, and F. Leroy, Surf. Sci. Rep. **64**, 255 (2009).
[32]M. Buljan, N. Radić, S. Bernstorff, G. Dražić, I. Bogdanović-Radović, and V. Holý, Acta. Cryst. A, in press (2011).
[33]M. Fanfoni and M. Tomellini, J. Phys. Cond. Mat. **17**, R571 (2005).
[34]F. S. Ham, J. Phys. Chem. Solids **6**, 335 (1958).
[35]R. Boistelle and J. P. Astier, J. Cryst. Growth **90**, 14 (1988).
[36]S. R. C. Pinto, A. G. Rolo, M. Buljan, A. Chahboun, S. Bernstorff, N. P. Barradas, E. Alves, R. J. Kashtiban, U. Bangert, and M. J. M. Gomes, Nanoscale Res. Lett. **6**, 341 (2011).
[37]M. Buljan *et al.* (in preparation).